

 Open access • Posted Content • DOI:10.1101/2020.09.04.283358

Unsupervised clustering analysis reveals global population structure of SARS-CoV-2 — Source link

Yawei Li, Qingyun Liu, Zexian Zeng, Yuan Luo

Institutions: Northwestern University, Harvard University

Published on: 04 Sep 2020 - bioRxiv (Elsevier Inc.)

Topics: Population and Cluster analysis

Related papers:

- [Clustering analysis of single nucleotide polymorphism data reveals population structure of SARS-CoV-2 worldwide](#)
- [Comparative genomics provides an operational classification system and reveals early emergence and biased spatio-temporal distribution of SARS-CoV-2](#)
- [Comparative genomic provides an operational classification system and reveals early emergence and spatio-temporal](#)
- [Using image-based haplotype alignments to map global adaptation of SARS-CoV-2](#)
- [Clustering Based Identification of SARS-CoV-2 Subtypes.](#)

Share this paper:    

View more about this paper here: <https://typeset.io/papers/unsupervised-clustering-analysis-reveals-global-population-yzpr1y4szw>

1 **Unsupervised clustering analysis reveals global population structure of SARS-**
2 **CoV-2**

3
4 Yawei Li¹, Qingyun Liu², Zexian Zeng³, Yuan Luo^{1*}

5
6 ¹ Department of Preventive Medicine, Northwestern University, Feinberg School of Medicine, Chicago, IL 60611, USA

7 ² Department of Immunology and Infectious Diseases, Harvard T. H. Chan School of Public Health, Boston, MA 02115,

8 USA.

9 ³ Department of Data Science, Dana Farber Cancer Institute, Harvard T.H. Chan School of Public Health, Boston, MA

10 02215, USA

11

12 * Corresponding author:

13 Email: yuan.luo@northwestern.edu

14

15 **Abstract**

16 Identifying the population structure of the newly emerged coronavirus SARS-CoV-2 has significant potential to inform
17 public health management and diagnosis. As SARS-CoV-2 sequencing data accrued, grouping them into clusters is
18 important for organizing the landscape of the population structure of the virus. Since we have little prior information about
19 the newly emerged coronavirus, we applied a state-of-the-art unsupervised deep learning clustering algorithm to group
20 16,873 SARS-CoV-2 strains, which automatically enables the identification of spatial structure for SARS-CoV-2. A total
21 of six distinct genomic clusters were identified using mutation profiles as input features. The varied proportions of the six
22 clusters within different continents revealed specific geographical distributions. Comprehensive analysis indicated that
23 genetic factors and human migration played an important role in shaping the specific geographical distribution of
24 population. This study provides a concrete framework for the use of clustering methods to study the global population
25 structure of SARS-CoV-2. In addition, clustering methods can be used for future studies of variant population structures in
26 specific regions of these fast-growing viruses.

27

28 **Introduction**

29 The COVID-19 pandemic was caused by severe acute respiratory syndrome coronavirus 2 (SARS-CoV-2) ^{1,2}, and has
30 spread throughout the world. In an effort to understand the molecular characteristics of the virus, viral genomes have been
31 abundantly sequenced and presented at the Global Initiative on Sharing All Influenza Data (GISAID). As an emerging virus,
32 it is important to understand the genetic diversity, evolutionary trajectory and possible routes of transmission of SARS-
33 CoV-2 from its natural reservoir to humans. Most studies have looked into the aspects of real-world SARS-CoV-2 evolution
34 and strain diversification through phylogenetic trees ^{4, 5, 6}. Phylogenetic tree is a graph that shows the evolutionary
35 relationships among various biological entities based on their genetic closeness ^{7, 8}. The distances from one entity to the
36 other entities indicate the degree of relationships. However, as population genomic datasets grow in size, simply using
37 pairwise genetic distances cannot present an explicit structure of the total population in phylogenetic analysis. Grouping

38 similar entities into the same cluster and identifying the number of main subtypes (clusters) makes it easier to understand
39 the main characteristics of the population. Traditionally, using the distance matrix and the bifurcations between branches
40 of leaves on the phylogenetic tree, entities can be grouped into clusters. However, when the number of entities becomes
41 large, it is not easy to directly and accurately partition the clades in the phylogenetic tree.

42 In order to identify a better way to effectively group entities, clustering methods emerge as more productive and robust
43 solutions. The objective of clustering is automatically minimizing intra-cluster distances and maximizing inter-cluster
44 distances⁹. Accurate clustering helps to better understand the inner relationships between data and inform downstream
45 analysis. Clustering methods have been widely used as a good supplemental tool in phylogenetic analysis, including
46 phylogenetic tree construction^{10, 11, 12}, ancestral relationship identification¹³, evolutionary rate estimation^{14, 15}, gene
47 evolutionary mechanisms research¹⁶ and population structure analysis¹⁷.

48 Herein, to identify the population structure of the newly emerged coronavirus SARS-CoV-2, we took inspiration from
49 recent state-of-the-art deep embedding clustering method¹⁸ to group a total of 16,873 strains. Compared with traditional
50 methods, this deep learning clustering algorithm showed significant improvements in terms of both Silhouette score, sum
51 of squared errors (SSE) and Bayesian information criterion (BIC)¹⁹. The clustering results showed that there were six
52 major clusters of SARS-CoV-2. In particular, we found that the proportions of six clusters in each continent showed a
53 specific geographical distribution. Our analysis revealed that the unique geographical distributions across the clusters are
54 both influenced by intrinsic genetic factors and migration of humans. This study provides a perspective of the SARS-CoV-2
55 population structural analysis, helping to investigate the evolution and spread of the virus across the human populations
56 worldwide.

57

58 **Results**

59 **Genetic analysis indicates high diversity and rapidly proliferating of SARS-CoV-2**

60 We obtained a total of 16,873 (98 from Africa, 1324 from Asia, 9527 from Europe, 4765 from North America, 1040 from

61 Oceania and 119 from South America) earliest SARS-CoV-2 whole-genome sequencing data from GISAID, aligned the
62 sequences, and identified the genetic variants. A total of 7,970 substitutions were identified, including 4,908 non-
63 synonymous mutations, 2,748 synonymous mutations and 314 intronic mutations. The average mutation count per genome
64 was 6.99 (Figure S1). The frequency spectrum of substitutions illustrated that more than half (54.05%) of the mutations
65 were singletons and 15.35% were doubletons. The proportion of the mutations below 0.01 was 99.28% (Figure S2). The
66 high percentage of these low-frequency mutations suggested that SARS-CoV-2 occurred recently and displayed a rapidly
67 proliferating pattern²⁰. In addition, there were 8,706 unique strains across the 16,873 strains (Figure S3), and most unique
68 strains (7,078) were singletons, yielding high diversity of the virus. In particular, Simpson's diversity index of the strains
69 was 0.8222, indicating that two random strains would have a high probability of being genetically different. The frequency
70 spectrum of substitutions and high Simpson's diversity index indicated high genetic diversity of SARS-CoV-2.

71

72 **Clustering of SARS-CoV-2 reveals six major clusters**

73 To clarify the main population structure of the virus, grouping these strains into clusters is necessary, as these clusters
74 displayed the major types of the virus. However, the genetic analysis of SARS-CoV-2 showed that there were 8,706 unique
75 strains across the 16,873 strains (Figure S3), it is not easy to directly and accurately partition the strains. For this reason,
76 we applied clustering techniques to measure similarities between these strains and effectively group them.

77 Because SARS-CoV-2 exhibits a limited number of SNPs per virus strain and little ongoing horizontal gene exchange,
78 making SNPs ideal clustering input features. We first used the aggregated SNP matrix to cluster samples using an
79 unsupervised deep learning clustering algorithm¹⁸ (see Methods). The unsupervised deep learning clustering algorithm
80 requires one to pre-specify the number of clusters (K), but we have little prior knowledge about the number of subtypes
81 formed by the heterogeneous SARS-CoV-2 genome. To determine the number of clusters, we plotted the curves of the SSE
82 and BIC under different cluster numbers ranging from 2 to 20 (Figure S4). We used the elbow method and chose the elbow
83 of the curve as the number of clusters²¹. This approach resulted in $K=6$ for both the SSE and BIC curves. To evaluate the

84 performance of the algorithm, we also employed K-means clustering²², hierarchical clustering and BIRCH clustering^{23, 24}
85 for comparison. The objective of clustering is minimizing intra-cluster distances and maximizing inter-cluster distances.
86 To this end, we did five repetitions for each of the four clustering algorithms and selected the one that achieved the best
87 performance (lowest average intra-cluster pairwise genetic distances). The average intra-cluster pairwise genetic distances
88 in the deep learning clustering algorithm (4.892) was significantly lower than that in K-means (4.896, P-value < 0.001,
89 Wilcoxon rank-sum test), hierarchical clustering (5.062, P-value < 0.001, Wilcoxon rank-sum test) and BIRCH (4.985, P-
90 value < 0.001, Wilcoxon rank-sum test). We compared the Silhouette score (Figure 1A), SSE (Figure 1B) and BIC (Figure
91 1C) of the four algorithms. The deep learning clustering obtained the highest Silhouette score and BIC, and the lowest SSE,
92 indicating that the clustering results of deep learning clustering are better than the other algorithms. In contrast, BIRCH
93 performed the worst of the four algorithms. We aligned the partitions of the six clusters against the phylogenetic tree for
94 the three best methods (Figure 1D). The clustering results indicated that the partitions from the three algorithms were
95 similar. The differences between the hierarchical clustering results and the two other clustering results were mainly at the
96 boundary of the clusters. Of the three methods, strains grouped by deep learning clustering and K-means were more
97 compact in the phylogenetic tree than those by hierarchical clustering. For example, the strains in both deep learning
98 clustering cluster D and K-means cluster D were split into two clusters using hierarchical clustering. However, such a split
99 was not supported by the phylogenetic tree (Figure 1D).

100 In the meantime, we used complementary approaches to validate the deep learning clustering results. First, we
101 compared the pairwise genetic distances between intra-cluster and inter-cluster. In all six clusters, the average number of
102 intra-cluster genetic distances was significantly lower (P-value < 0.001, Wilcoxon rank-sum test, Figure 1E) than inter-
103 cluster genetic distances. Next, we applied T-distributed Stochastic Neighbor Embedding (t-SNE) to visualize the deep
104 learning clustering results. In the t-SNE plot, the strains were adequately isolated between clusters (Figure 1F).

105

106 **The varied proportions of the clusters in different continents**

107 Mapping the proportions of strains from each continent showed that the clusters differed in their geographical distributions
108 (Figure 2, Table S1). Of the six clusters, cluster C spread globally. By contrast, cluster A and cluster F occurred at high
109 frequencies in specific regions. 81.92% of the strains in cluster A and 85.73% of the strains in cluster F were from Europe.
110 The geographical spread of each of the three remaining clusters was intermediate. Cluster E occurred at higher frequencies
111 in North America and Europe, and lower frequencies in Asia and Oceania. Cluster D occurred at higher frequencies in
112 North America, and lower frequencies in Asia, Europe and Oceania. The strains in cluster B were mainly in Asia and Europe
113 and partially in North America and Oceania.

114 However, due to the sampling bias of the SARS-CoV-2, 85% of the strains were collected from Europe and North
115 America (Table S1), making the proportion of the continents in each cluster not informative. Therefore, we evaluated the
116 proportion of the clusters on each continent. In most continents, the distributions of the strains were concentrated in one or
117 two clusters, including Asia (49% in cluster B), Africa (66% in cluster C), South America (78% in cluster C and F), North
118 America (74% in cluster D and E) and Europe (64% in cluster C and F). Strikingly, Oceania was the only continent that
119 was uniformly separated into the six clusters, indicating strains in Oceania were more diverse than in the other continents.

120 The different geographical distributions for the six clusters could be due to intrinsic genetic factors, extrinsic factors
121 such as the migration of humans, or both. Hence, we next aimed to explore the genomic characteristics of these clusters,
122 as well as the transmission and human migration of the virus across the globe.

124 **The genetic variance analyses indicated high diversity between clusters**

125 If the different geographical distributions for the six clusters were due to intrinsic genetic factors, there would be high
126 genetic variance between the clusters. The average mutation counts for the six clusters were 6.38, 3.49, 6.57, 7.09, 7.89
127 and 8.96 (Figure S5), respectively. Considering the different collection dates (Figure 3A) of the strains, mutation rates as
128 opposed to mutation counts were more effective for describing the genetic variations between clusters. We defined the date
129 when the reference strain was collected as the index date. The average mutation rates for the six clusters were 25.55, 15.91,

130 25.44, 31.64, 30.99 and 34.12 substitutions per year, respectively. Specifically, the average mutation rate in cluster B was
131 significantly lower (P-value < 0.001, Wilcoxon rank-sum test) than those in other clusters. In contrast, the average mutation
132 rate in cluster F was significantly higher (P-value < 0.001, Wilcoxon rank-sum test) than those in other clusters. The
133 Simpson's diversity indexes for the six clusters were 0.7616, 0.7608, 0.8398, 0.8466, 0.8082 and 0.8502, respectively. Both
134 the average mutation rate and Simpson's index were highest in cluster F, suggesting that the diversity of cluster F was
135 higher than the other clusters. The nucleotide diversity per site for the six clusters was 0.0196%, 0.0222%, 0.0171%,
136 0.0256%, 0.0131% and 0.0132%. The high mutation rates but low nucleotide diversity in cluster E and cluster F suggests
137 that these two clusters may have more fixed mutations than the other clusters. The nucleotide diversity of each gene across
138 all clusters is displayed in Figure 3B-G. Except for some short genes that are unlikely to be informative, the diversity of
139 most genes was close to the diversity of their genome-wide variants. Our analysis showed that intra-cluster genetic diversity
140 differed between clusters, suggesting that selective pressures were different between clusters. These different selective
141 pressures will affect the geographical distribution of each cluster.

142

143 **Explore mutations that shaped the geographical distribution of population structure.**

144 The high genetic diversity between clusters indicated that the frequencies of the mutations across clusters were very
145 different. In order to explore whether there are mutations that affect the genetic structure within the clusters, we applied
146 ANOVA to identify the statistically significant mutations that were strongly associated with clusters. Across the 7,970
147 substitutions, 26.27% (2,094 substitutions) of them achieved P-values < 0.05 (Figure S6). We found that some of these
148 mutations were fixed in one or several clusters. Cluster C, cluster E and cluster F shared four common fixed substitutions:
149 A23403G, C241T, C3037T and C14408T. Cluster E had two additional fixed substitutions: C1059T and G25563T, and
150 cluster F had three additional substitutions from position 28,881 to position 28,883. For the remaining three clusters, there
151 were two fixed substitutions (C8782T, T28144C) and three fixed substitutions (G11083T, G14805T and G26144T) in
152 cluster A. It is noteworthy that the fixed mutation numbers in cluster E (six) and cluster F (seven) were higher than in any

153 of the other clusters, which was consistent with our conclusion of the high mutation rates but low nucleotide diversity in
154 cluster E and cluster F.

155 We selected the 2% (42/2094) substitutions that achieved the lowest P-values (Table 1) and analyzed their distributions
156 in the clusters. Of the 42 substitutions, there were 26 nonsynonymous mutations (mutation G28882A was in a trinucleotide
157 mutation from position 28881 to 28883 that spans two codons and results in an RG (arginine-glycine) to KR (lysine-
158 arginine) amino acid change). We focused on these nonsynonymous mutations as these mutations may be under selection
159 that affect the population structure²⁵. Some of these substitutions were reported to impact the evolution of SARS-CoV-2
160^{26,27}. For example, mutation A23403G (D614G, Aspartic acid to Glycine) in the *spike* protein domains was reported to show
161 significant variation in cytopathic effects and viral load, and substantially change the pathogenicity of SARS-CoV-2²⁸.
162 This mutation was accompanied by a mutation (T14408C) that results in an RNA-dependent RNA polymerase (RdRp)
163 amino acid change²⁹. In addition, Tang et al³⁰ used mutation T28144C to define “L” type (defined as “L” type because
164 T28,144 is in the codon of Leucine) and “S” type (defined as “S” type because C28,144 is in the codon of Serine) of SARS-
165 CoV-2. They found that the “L” type was more transmissible and aggressive than the “S” type.

166 Previous studies have reported that recombination is common in coronavirus^{4,31,32}. Given that recombinations in
167 SARS-CoV-2 may perturb the clustering, we used Haploview³³ to analyze the linkage disequilibrium (LD) by calculating
168 standardized disequilibrium coefficients (D') and squared allele-frequency correlations (r^2) of the 42 substitutions. D' is
169 affected solely by recombination and not by differences in allele frequencies between sites, and r^2 is also affected by
170 differences in allele frequencies at the two sites. In the heatmap of D' and r^2 (Figure S7), no obvious LD blocks were
171 discovered, indicating that our clustering of SARS-CoV-2 strains using substitutions was not distorted by recombination.

172 Selection usually affects the distribution of the mutations in the population. Purifying selection tends to remove amino
173 acid-altering mutations, while positive selection tends to increase the frequency of the mutations. Considering the rapidly
174 proliferating pattern of SARS-CoV-2 that strengthened the power of drift relative to the power of purifying selection^{34,35},
175³⁶, we mainly focused on the positive selective sites. We applied HyPhy³⁷ to infer the probabilities of the extracted 26

176 nonsynonymous mutations that were under positive selection. There are nine mutations (asterisks in Table 1) with a positive
177 probability >0.95 . In particular, mutations G2891A, G11083T, C14408T, C17747T and A23403G (D614G) were reported
178 as recurrent mutations^{26,38}. The recurrence of these mutations agrees with the assumption that they may confer selective
179 advantages in the population. These possible positively selected mutations may result in greater diversity among clusters
180 with different population structures of SARS-CoV-2 across geographical regions.

181

182 **The global spread of SARS-CoV-2**

183 Regardless of the genetic factors, the travel of humans could also lead to unique geographical distributions in today's highly
184 globalized world. By analyzing the frequencies of the extracted 42 mutations in each cluster (Figure 4A) and their collected
185 daily counts (Figure 4B), we can trace the dynamics of substitutions in the SARS-CoV-2 genome. The four genetically
186 linked mutations, A23403G (D614G), C241T, C3037T and C14408T that were fixed across three clusters (C, E and F) had
187 become the highest frequency mutations in the world, with a high frequency on all continents in our downloaded sequences,
188 including South America (87%), Africa (86%), Europe (75%), North America (65%), Oceania (55%) and Asia (32%). The
189 earliest time when sequences carrying these mutations was collected was in late January 2020. About a month later, these
190 mutations were discovered worldwide. Though the mutation A23403G (D614G) has been reported and estimated to be a
191 positive selective mutation, it is almost impossible to spread to the world without human migration in such a short time.
192 Besides these high frequency mutations, some lower frequency mutations also provided some evidence of human migration.
193 We explored the geographical distributions of mutations with global frequencies <0.05 in Table 1. Though most of these
194 low frequency mutations were mainly collected within a single continent, we still find two mutations, T28688C and
195 G1397A, were discovered in Asia, Europe and Oceania with high proportion. In addition, the spatial geographical
196 distributions of some substitutions also provide the evidence that human migration may have influenced the spread of the
197 virus. For example, on the west coast of the USA, most strains accumulated the mutations C8782T and T28144C (cluster
198 D), and these mutations were also found in high frequencies in east Asia. In contrast, on the east coast of the USA, most

199 strains accumulated the mutations A23403G, C241T, C3037T, C14408T, C1059T and G25563T (cluster E), and the similar
200 strains were mainly discovered in Europe (Figure S8).

201

202 **Discussion**

203 Understanding the population structure of SARS-CoV-2 is important in evaluating future risks of novel infections. To
204 precisely analyze their population structure, we used clustering methods in phylogenetic analysis to group a total of 16,873
205 publicly available SARS-CoV-2 strains. To improve the accuracy, we use a state-of-the-art deep learning clustering
206 algorithm, which has been demonstrated to exhibit better performance than three traditional clustering algorithms: K-means
207 clustering, hierarchical clustering and BIRCH.

208 Our clustering results indicated six major clusters of SARS-CoV-2. The mutation profile characterizing clusters of the
209 viral sequences displayed specific geographical distributions. Most continents were mainly concentrated in one or two
210 clusters, but we also found that in Oceania, the strains were uniformly separated across the six clusters. To evaluate whether
211 the geographical distributions for the clusters were due to genetic factors or travel of humans. The varied intra-cluster
212 genetic diversity across the clusters suggested different selective pressures between clusters, which would affect the
213 geographical distributions across the clusters. By analyzing the statistically significant mutations that were strongly
214 associated with the clusters we identified that some mutations might be under positive selection, indicating different
215 geographical distributions between the clusters were partially affected by these mutations. In addition, the dynamics and
216 the spatial geographical distributions of some substitutions suggested that human migration may also have affected the
217 different geographical distributions. In general, our findings indicate that the geographical distributions for the clusters are
218 the result of both genetic factors and migration of humans.

219 It is noteworthy that our study is limited due to the sampling bias of SARS-CoV-2, with more than 60% of the strains
220 being from the United Kingdom and the USA. In contrast, the overall proportion of strains from Africa and South America
221 is less than 2% (Table S1). Sampling biases can lead to biased parameter estimation and affect the clustering results we

222 observed. For example, the frequency of mutation C15324T reached 41.84% in Africa, but was only 2.21% outside Africa.
223 The frequency of mutation T29148C reached 15.13% in South America, but was only 0.12% outside South America.
224 Another mutation T27299C with frequency 10.92% in South America was only found with frequency 0.08% in other
225 regions. In fact, all three mutations were mostly grouped in single clusters, indicating these mutations were highly
226 concentrated. However, due to the small proportion of the strains from these two continents, these mutations were unable
227 to affect the clustering of samples. To address this issue, more strains were needed to be collected from these continents.
228 In addition, we found that in cluster B, there were no fixed mutations. We calculated the pairwise dependency scores (see
229 Methods) of all the mutations with frequencies >0.05 in cluster B and discovered five main subclusters (Figure S9). Other
230 than the mutation G11083T that was discovered in two subclusters, there were no common mutations between either of the
231 five clusters. As shown in Figure 3A, these strains were grouped in one cluster mainly because these strains had smaller
232 mutation counts than strains in other clusters. The genetic distance between two strains was still small, though they shared
233 no common mutations. To address this issue, another clustering can be used for more further analyses.

234 Despite the limited number of SARS-CoV-2 genome sequences, our analysis of population genetics is formative. Our
235 discovery of high genetic diversity in SARS-CoV-2 is consistent with an earlier study³⁹. The topology and the divergence
236 of the clusters in the phylogenetic tree illustrate a relatively recent common ancestor, similar to the fact that the emergence
237 and the spread of the virus was highly concentrated in a short time^{2, 40, 41, 42}. Our work, as well as previous studies^{43, 44} that
238 use clustering techniques to study the population structure of the SARS-CoV-2 virus, has proved to be a valuable
239 supplemental tool in phylogenetic analyses. In addition, clustering ideas can be used for further study of variant population
240 structures in specific regions of these fast-growing viruses.

241

242 **Methods**

243 **SARS-CoV-2 sample collection**

244 A set of African, Asian, European, North American, Oceanian and South American SARS-CoV-2 strains marked as “high

245 coverage” were downloaded from GISAID. The “high coverage” was defined as strains with <1% Ns and <0.05% unique
246 amino acid mutations (not seen in other sequences in databases) and no insertion/deletion unless verified by the submitter.
247 In addition, all strains with a non-human host and all assemblies of total genome length less than 29,000 bps were removed
248 from our analysis. Ultimately, our dataset consisted of 16,873 strains.

249

250 **Mutation calls and phylogenetic reconstruction**

251 All downloaded genomes were mapped to the reference genome of SARS-CoV-2 (GenBank Accession Number:
252 NC_045512.2) following Nextstrain pipeline ⁴⁵. Multiple sequence alignments and pairwise alignments were constructed
253 using CLUSTALW 2.1 ⁴⁶. Considering many putatively artefactual mutations and the gaps in sequences are located at the
254 beginning and end of the alignment, we masked the first 130 bps and last 50 bps in mutation calling following Nextstrain
255 pipeline. We used substitutions as features to reconstruct the phylogenetic tree using FastTree 2 ⁴⁷. The phylogeny is rooted
256 following Nextstrain pipeline using FigTree v1.4.4. The phylogenetic trees were visualized using the online tool Interactive
257 Tree Of Life (iTOL v5) ⁴⁸.

258

259 **Region analysis and data visualization**

260 For each country with SARS-CoV-2 data available, clustering proportions were calculated and plotted on the world map
261 using the tool Tableau Desktop 2020.2. Other Figures and statistical analyses were generated by the ggplot2 library in R
262 3.6.1, the seaborn package in Python 3.7.6 and GraphPad Prism 8.0.2.

263

264 **Data clustering**

265 Herein, we employed a deep learning unsupervised clustering algorithm to iteratively cluster the SARS-CoV-2 strains ¹⁸.
266 Each identified cluster was considered to be a subtype of SARS-CoV-2. We first used K-means clustering to initialize
267 centroids for the clusters. To determine the number of clusters, we plotted the curves of the sum of squared errors (SSE)

268 and Bayesian information criterion (BIC) ¹⁹ under different cluster numbers ranging from 2 to 20.

269 To update the cluster assignments, we implemented the Student's t-distribution as a kernel to measure the distance
270 from a strain (h_i) to a cluster centroid (u_j):

$$271 \quad q_{ij} = \frac{(1 + \|h_i - u_j\|^2 / \alpha)^{-\frac{\alpha+1}{2}}}{\sum_{j'=1}^K (1 + \|h_i - u_{j'}\|^2 / \alpha)^{-\frac{\alpha+1}{2}}}$$

272 where the distance q_{ij} can be interpreted as the probability of assigning strain i to cluster j . The α is the degree of freedom
273 of the Student's t-distribution, and we let $\alpha = 1$ in this study. Next, we defined an auxiliary target distribution P by raising
274 each q_{ij} to the second power which upweights strains assigned with high confidence:

$$275 \quad p_{ij} = \frac{q_{ij}^2 / \sum_{i=1}^N q_{ij}}{\sum_{j'=1}^K (q_{ij'}^2 / \sum_{i=1}^N q_{ij'})}$$

276 where the denominator is to normalize the loss contribution of each centroid to prevent large clusters from distorting the
277 feature space. Finally, we defined the objective function using a Kullback-Leibler (KL) divergence loss:

$$278 \quad L = \text{KL}(P||Q) = \sum_{i=1}^N \sum_{j=1}^K p_{ij} \log \frac{p_{ij}}{q_{ij}}$$

279 The parameters and cluster centroids were jointly optimized by minimizing L using Stochastic Gradient Descent (SGD)
280 with momentum.

281 Besides the deep learning clustering algorithm, we also employed K-means clustering, hierarchical clustering and
282 BIRCH (Balanced Iterative Reducing and Clustering using Hierarchies) for SARS-CoV-2 strain clustering. The three
283 models were implemented using the Python package sklearn with the KMeans function, AgglomerativeClustering function
284 and Birch function, respectively.

285

286 **Simpson's diversity index**

287 Simpson's Diversity Index (D) is a measure of diversity that considers the number of entities as well as their abundance.
288 The index measures the probability that two randomly selected individuals are the same. The formula to calculate the value
289 of the index is:

290
$$D = 1 - \frac{\sum_{all\ traits} n(n-1)}{N(N-1)}$$

291 where n is the number of individuals displaying one trait and N is the total number of all individuals. The value of D ranges
292 between 0 and 1. With this index, 1 represents infinite diversity and 0 denotes no diversity.

293

294 **Inferring positive/purifying selection of individual sites**

295 To test which position was under selective pressure, we used a set of programs available in HyPhy to calculate
296 nonsynonymous (dN) and synonymous (dS) substitution rates on a per-site basis to infer pervasive selection. Fast
297 Unconstrained Bayesian AppRoximation (FUBAR) was applied to detect overall sites under positive selection. The
298 positively selected sites were identified using a probability larger than 0.95 using the FUBAR method.

299

300 **Pairwise mutation dependency score**

301 Pairwise mutation dependency scores can measure the order in which genetic mutations are acquired within a cluster. For
302 two selected mutations X and Y, the score $S(X|Y)$ represents the proportion of strains that accumulated both X among the
303 strains that accumulated mutation Y. $S(X|Y)$ and $S(Y|X)$ can be calculated using the following functions:

304
$$S(X|Y) = \frac{\sum_{all\ samples} S_X = 1 \ \& \ S_Y = 1}{\sum_{all\ samples} S_Y = 1}$$

305
$$S(Y|X) = \frac{\sum_{all\ samples} S_X = 1 \ \& \ S_Y = 1}{\sum_{all\ samples} S_X = 1}$$

306 where $S_X = 1$ denotes that the sequence has a mutation X. Pairwise mutation dependency score displays the correlation
307 and the timescale relationship of the two mutations. The value of $S(X|Y)$ and $S(Y|X)$ ranges between 0 and 1. With this
308 index, $S(X|Y) = 1$ with $S(Y|X) < 1$ represents that mutation Y occurs after mutation X. In contrast, $S(X|Y) = 1$ with $S(Y|X)$
309 $= 1$ represents that the two mutations occur simultaneously and are genetically linked. Statistical analyses and data
310 presentations were generated using Python 3.7.6.

311

312 **Data Availability**

313 The publicly available SARS-CoV-2 datasets in this study are available at GISAID (<https://www.gisaid.org>). The reference
314 SARS-CoV-2 is available at the NCBI GenBank (GenBank Accession Number: NC_045512.2,

315 https://www.ncbi.nlm.nih.gov/nuccore/NC_045512.2).

316

317 **References**

- 318 1. Coronaviridae Study Group of the International Committee on Taxonomy of V. The species Severe acute
319 respiratory syndrome-related coronavirus: classifying 2019-nCoV and naming it SARS-CoV-2. *Nat Microbiol* **5**,
320 536-544 (2020).
- 321 2. Zhu N, *et al.* A Novel Coronavirus from Patients with Pneumonia in China, 2019. *N Engl J Med* **382**, 727-733
322 (2020).
- 323 3. Li R, *et al.* Substantial undocumented infection facilitates the rapid dissemination of novel coronavirus (SARS-
324 CoV-2). *Science* **368**, 489-493 (2020).
- 325 4. Rehman SU, Shafique L, Ihsan A, Liu Q. Evolutionary Trajectory for the Emergence of Novel Coronavirus SARS-
326 CoV-2. *Pathogens* **9**, (2020).
- 327 5. Forster P, Forster L, Renfrew C, Forster M. Phylogenetic network analysis of SARS-CoV-2 genomes. *Proc Natl*
328 *Acad Sci U S A* **117**, 9241-9243 (2020).
- 329 6. Koyama T, Platt D, Parida L. *Variant analysis of COVID-19 genomes* (2020).
- 330 7. Mahapatro G, Mishra D, Shaw K, Mishra S, Jena T. Phylogenetic Tree Construction for DNA Sequences using
331 Clustering Methods. *Procedia Engineer* **38**, 1362-1366 (2012).
- 332 8. Sharma A, Jaloree S, Thakur R. Review of Clustering Methods: Toward Phylogenetic Tree Constructions. 475-
333 480 (2018).
- 334 9. Gonzalez TF. Clustering to minimize the maximum intercluster distance. *Theoretical Computer Science* **38**, 293-
335 306 (1985).
- 336 10. Wang J, Soininen J, He J, Shen J. Phylogenetic clustering increases with elevation for microbes. *Environ Microbiol*
337 *Rep* **4**, 217-226 (2012).

- 338 11. Ning J, Beiko RG. Phylogenetic approaches to microbial community classification. *Microbiome* **3**, 47 (2015).
- 339 12. Fioravanti D, *et al.* Phylogenetic convolutional neural networks in metagenomics. *BMC Bioinformatics* **19**, 49
340 (2018).
- 341 13. Qin L, Chen YX, Pan Y, Chen L. A novel approach to phylogenetic tree construction using stochastic optimization
342 and clustering. *Bmc Bioinformatics* **7**, (2006).
- 343 14. Felsenstein J, Churchill GA. A hidden Markov Model approach to variation among sites in rate of evolution. *Mol*
344 *Biol Evol* **13**, 93-104 (1996).
- 345 15. Siepel A, *et al.* Evolutionarily conserved elements in vertebrate, insect, worm, and yeast genomes. *Genome Res*
346 **15**, 1034-1050 (2005).
- 347 16. Medema MH, Cimermancic P, Sali A, Takano E, Fischbach MA. A systematic computational analysis of
348 biosynthetic gene cluster evolution: lessons for engineering biosynthesis. *PLoS Comput Biol* **10**, e1004016 (2014).
- 349 17. Han E, *et al.* Clustering of 770,000 genomes reveals post-colonial population structure of North America. *Nat*
350 *Commun* **8**, 14238 (2017).
- 351 18. Xie J, Girshick R, Farhadi A. Unsupervised deep embedding for clustering analysis. In: *Proceedings of the 33rd*
352 *International Conference on International Conference on Machine Learning - Volume 48*. JMLR.org (2016).
- 353 19. Schwarz G. Estimating the Dimension of a Model. *Ann Statist* **6**, 461-464 (1978).
- 354 20. Yu WB, Tang GD, Zhang L, Corlett RT. Decoding the evolution and transmissions of the novel pneumonia
355 coronavirus (SARS-CoV-2 / HCoV-19) using whole genomic data. *Zool Res* **41**, 247-257 (2020).
- 356 21. Thorndike RL. Who Belongs in the Family? *Psychometrika* **18**, 267-276 (1953).
- 357 22. MacQueen J. Some methods for classification and analysis of multivariate observations. In: *Proceedings of the*
358 *Fifth Berkeley Symposium on Mathematical Statistics and Probability, Volume 1: Statistics*. University of
359 California Press (1967).
- 360 23. Zhang T, Ramakrishnan R, Livny M. BIRCH: an efficient data clustering method for very large databases. In:

- 361 *Proceedings of the 1996 ACM SIGMOD international conference on Management of data*. Association for
362 Computing Machinery (1996).
- 363 24. Zhang T, Ramakrishnan R, Livny M. BIRCH: A New Data Clustering Algorithm and Its Applications. *Data*
364 *Mining and Knowledge Discovery* **1**, 141-182 (1997).
- 365 25. Hartl DL, Clark AG. *Principles of population genetics*, 4th edn. Sinauer Associates (2007).
- 366 26. van Dorp L, *et al.* Emergence of genomic diversity and recurrent mutations in SARS-CoV-2. *Infect Genet Evol*
367 **83**, 104351 (2020).
- 368 27. Yin C. Genotyping coronavirus SARS-CoV-2: methods and implications. *Genomics*, (2020).
- 369 28. Yao H, *et al.* Patient-derived mutations impact pathogenicity of SARS-CoV-2. *medRxiv*,
370 2020.2004.2014.20060160 (2020).
- 371 29. Korber B, *et al.* Tracking Changes in SARS-CoV-2 Spike: Evidence that D614G Increases Infectivity of the
372 COVID-19 Virus. *Cell* **182**, 812-+ (2020).
- 373 30. Tang X, *et al.* On the origin and continuing evolution of SARS-CoV-2. *National Science Review*, (2020).
- 374 31. Graham RL, Baric RS. Recombination, reservoirs, and the modular spike: mechanisms of coronavirus cross-
375 species transmission. *J Virol* **84**, 3134-3146 (2010).
- 376 32. Rouchka E, Chariker J, Chung D. Phylogenetic and Variant Analysis of 1,040 SARS-CoV-2 Genomes. (2020).
- 377 33. Barrett JC, Fry B, Maller J, Daly MJ. Haploview: analysis and visualization of LD and haplotype maps.
378 *Bioinformatics* **21**, 263-265 (2005).
- 379 34. Nowak MA, Michor F, Iwasa Y. The linear process of somatic evolution. *Proc Natl Acad Sci U S A* **100**, 14966-
380 14969 (2003).
- 381
- 382 35. Wu CI, Wang HY, Ling S, Lu X. The Ecology and Evolution of Cancer: The Ultra-Microevolutionary Process.
383 *Annu Rev Genet* **50**, 347-369 (2016).

- 384 36. Chen Y, Tong D, Wu CI. A New Formulation of Random Genetic Drift and Its Application to the Evolution of Cell
385 Populations. *Mol Biol Evol* **34**, 2057-2064 (2017).
- 386 37. Pond SLK, *et al.* HyPhy 2.5-A Customizable Platform for Evolutionary Hypothesis Testing Using Phylogenies.
387 *Mol Biol Evol* **37**, 295-299 (2020).
- 388 38. Pachetti M, *et al.* Emerging SARS-CoV-2 mutation hot spots include a novel RNA-dependent-RNA polymerase
389 variant. *J Transl Med* **18**, 179 (2020).
- 390 39. Li X, *et al.* Transmission dynamics and evolutionary history of 2019-nCoV. *J Med Virol* **92**, 501-511 (2020).
- 391 40. Chan JFW, *et al.* A familial cluster of pneumonia associated with the 2019 novel coronavirus indicating person-
392 to-person transmission: a study of a family cluster. *Lancet* **395**, 514-523 (2020).
- 393 41. Sun J, *et al.* COVID-19: Epidemiology, Evolution, and Cross-Disciplinary Perspectives. *Trends Mol Med* **26**, 483-
394 495 (2020).
- 395 42. Zhou P, *et al.* A pneumonia outbreak associated with a new coronavirus of probable bat origin. *Nature* **579**, 270-
396 273 (2020).
- 397 43. Mishra A, *et al.* Mutation landscape of SARS-CoV-2 reveals three mutually exclusive clusters of leading and
398 trailing single nucleotide substitutions. *bioRxiv*, 2020.2005.2007.082768 (2020).
- 399 44. Seemann T, *et al.* Tracking the COVID-19 pandemic in Australia using genomics. *Nature Communications* **11**,
400 4376 (2020).
- 401 45. Hadfield J, *et al.* Nextstrain: real-time tracking of pathogen evolution. *Bioinformatics* **34**, 4121-4123 (2018).
- 402 46. Larkin MA, *et al.* Clustal W and Clustal X version 2.0. *Bioinformatics* **23**, 2947-2948 (2007).
- 403 47. Price MN, Dehal PS, Arkin AP. FastTree 2--approximately maximum-likelihood trees for large alignments. *PLoS*
404 *One* **5**, e9490 (2010).
- 405 48. Letunic I, Bork P. Interactive Tree Of Life (iTOL): an online tool for phylogenetic tree display and annotation.
406 *Bioinformatics* **23**, 127-128 (2007).

407

408 **Competing Interests**

409 The authors declare no competing interests.

410

411 **Authors' contributions**

412 Y.Luo and Y.Li designed the research; Y.Li and Q.L. analyzed data; Y.Luo, Y.Li and Q.L. contributed to the theory; and

413 Y.Luo and Y.Li drafted the manuscript. All authors have read, edited and approved the final manuscript.

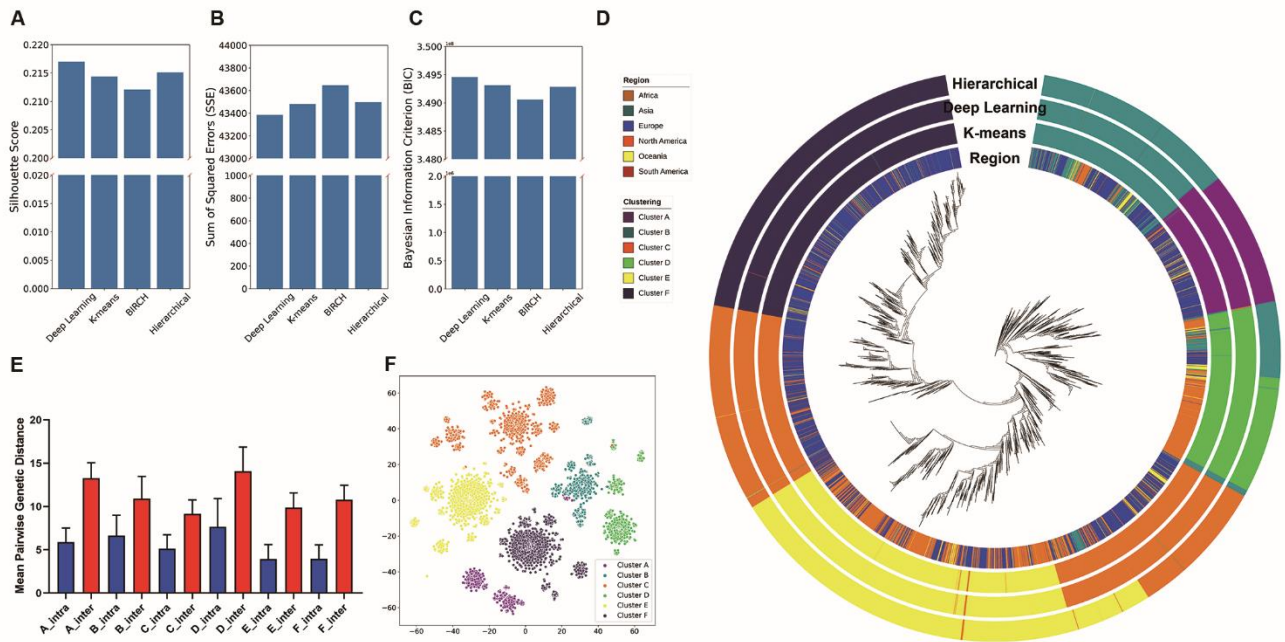
414

415 **Table 1.** The information of the 42 mutations using ANOVA.

Mutation	Substitution	Amino Acid Substitution	Type	GENE	Frequency	Cluster					
						A	B	C	D	E	F
C241T	C > T	Intron	Intron	Intron	66.37%	10	10	4238	2	3548	3391
T490A	T > A	D > E	N	ORF1ab	1.04%	0	0	1	174	0	0
T514C	T > C	H > H	S	ORF1ab	0.97%	0	162	1	0	0	0
C1059T*	C > T	T > I	N	ORF1ab	21.69%	1	8	2	0	3645	3
G1397A	G > A	V > I	N	ORF1ab	1.12%	0	186	0	0	1	2
G1440A	G > A	G > D	N	ORF1ab	1.92%	0	324	0	0	0	0
A2480G	A > G	I > V	N	ORF1ab	3.60%	608	0	0	0	0	0
C2558T	C > T	P > S	N	ORF1ab	3.83%	646	1	0	0	0	0
G2891A*	G > A	A > T	N	ORF1ab	1.77%	0	298	0	0	0	0
C3037T	C > T	F > F	S	ORF1ab	67.26%	2	7	4277	3	3611	3448
C3177T	C > T	P > L	N	ORF1ab	1.05%	0	0	1	171	6	0
C6312A	C > A	T > K	N	ORF1ab	1.14%	0	189	1	0	0	3
C8782T	C > T	S > S	S	ORF1ab	11.42%	1	21	5	1898	1	1
T9477A	T > A	F > Y	N	ORF1ab	1.17%	0	3	0	195	0	0
G11083T*	G > T	L > F	N	ORF1ab	11.81%	1342	485	52	21	54	39
C14408T*	C > T	P > L	N	ORF1ab	67.47%	1	8	4301	2	3636	3436
C14805T	C > T	Y > Y	S	ORF1ab	9.39%	1352	8	1	195	0	28
T17247C	T > C	R > R	S	ORF1ab	3.00%	500	5	1	0	0	0
C17747T*	C > T	P > L	N	ORF1ab	6.92%	1	0	0	1165	1	0
A17858G	A > G	Y > C	N	ORF1ab	7.05%	1	1	0	1187	0	0
C18060T	C > T	L > L	S	ORF1ab	7.16%	0	3	2	1202	1	0
T18736C	T > C	F > L	N	ORF1ab	1.01%	0	0	1	169	0	0
C18877T	C > T	L > L	S	ORF1ab	2.67%	2	2	440	4	0	2
A20268G	A > G	L > L	S	ORF1ab	4.61%	0	1	773	3	0	1
A23403G*	A > G	D > G	N	S	67.65%	4	4	4316	6	3634	3451
C23731T	C > T	T > T	S	S	1.68%	0	0	0	0	1	282
C23929T	C > T	Y > Y	S	S	1.13%	0	186	1	0	1	2
C24034T	C > T	N > N	S	S	1.16%	0	2	1	187	4	1
G25563T*	G > T	Q > H	N	ORF3a	26.44%	1	3	829	2	3625	2
G25979T	G > T	G > V	N	ORF3a	1.16%	0	2	1	193	0	0
G26144T*	G > T	G > V	N	ORF3a	8.61%	1387	62	0	1	1	1
T26729C	T > C	A > A	S	M	1.07%	0	1	1	179	0	0
C27046T	C > T	T > M	N	M	2.13%	0	1	5	0	0	353
G28077C	G > C	V > L	N	ORF8	1.13%	0	1	1	188	0	0
T28144C*	T > C	L > S	N	ORF8	11.36%	0	10	1	1903	2	0
C28657T	C > T	D > D	S	N	1.21%	0	3	3	196	1	2
T28688C	T > C	L > L	S	N	1.07%	0	178	1	0	1	0
C28863T	C > T	S > L	N	N	1.19%	1	2	2	193	2	0
G28881A	G > A	R > K	N	N	20.54%	4	3	3	1	1	3453
G28882A	G > A	R > K ¹	N	N	20.49%	1	2	0	0	0	3454
G28883C	G > C	G > R	N	N	20.49%	1	2	1	0	0	3453
A29700G	A > G	Intron	Intron	Intron	1.04%	0	0	4	167	4	1

416 ¹ G28881A and G28882A occur within the same codon. Amino acid annotation (R > K) is based on the co-occurrence of
417 these mutations.

418 * Under positive selection inferred by HyPhy.



419

420 **Figure 1. Clustering of SARS-CoV-2.** (A, B and C) The Silhouette score (A), Sum of Squared Errors (SSE; B) and

421 Bayesian Information Criterion (BIC; C) for the four selected algorithms (X axis). (D) Phylogenetic tree of 16,873 SARS-

422 CoV-2 strains. Four colored panels outside the phylogenetic tree are used to identify auxiliary information for each virus

423 strain. The inner panel represents the distribution of the continents. The outer three panels represent the partitions of the

424 six clusters across the three best performance clustering algorithms (deep learning, K-means and Hierarchical) in the tree.

425 (E) Mean pairwise genetic distances for intra-clustered and inter-clustered genetic distances. The blue bars represent mean

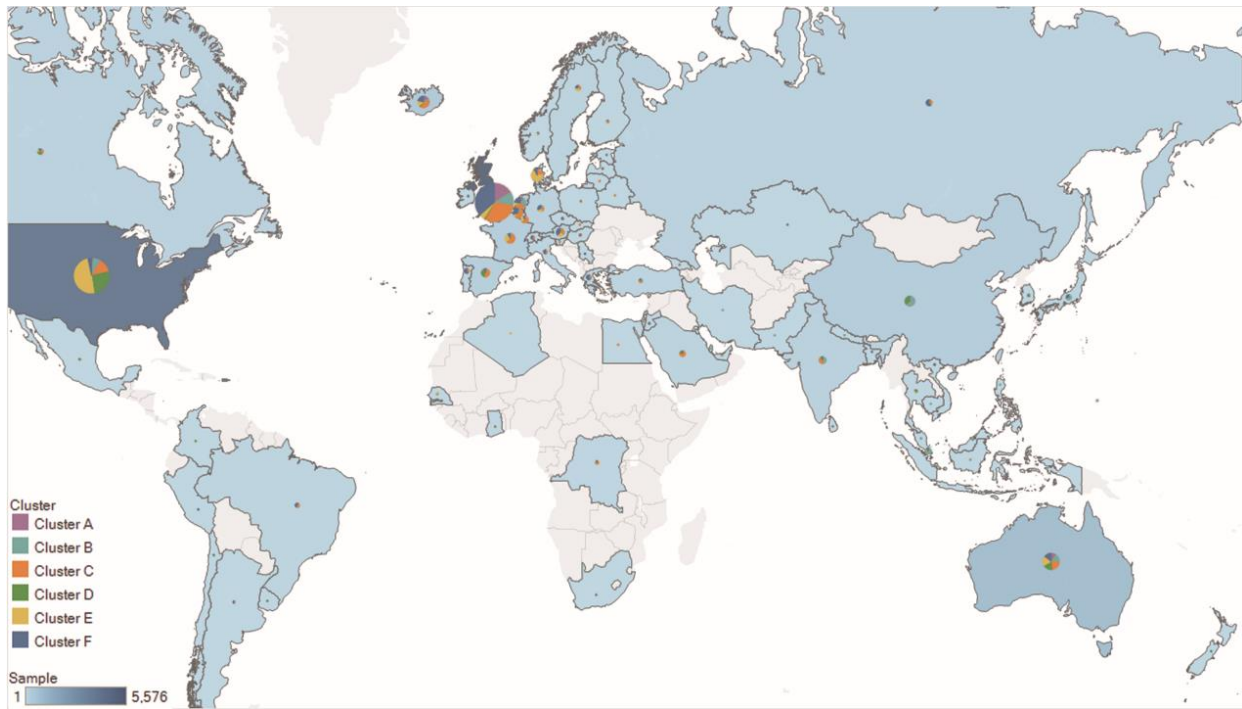
426 pairwise genetic distances between pairs of isolates within the clusters, and the red bars represent mean pairwise genetic

427 distances between pairs of isolates outside the clusters. The error bar represents the standard deviation. The mean distance

428 between pairs of strains for intra-clusters was significantly lower (P-value < 0.001, Wilcoxon rank-sum test) than that of

429 inter-clusters. (F) The t-SNE plot of the deep learning clustering results. Each dot represents one strain and each color

430 represents the corresponding cluster.

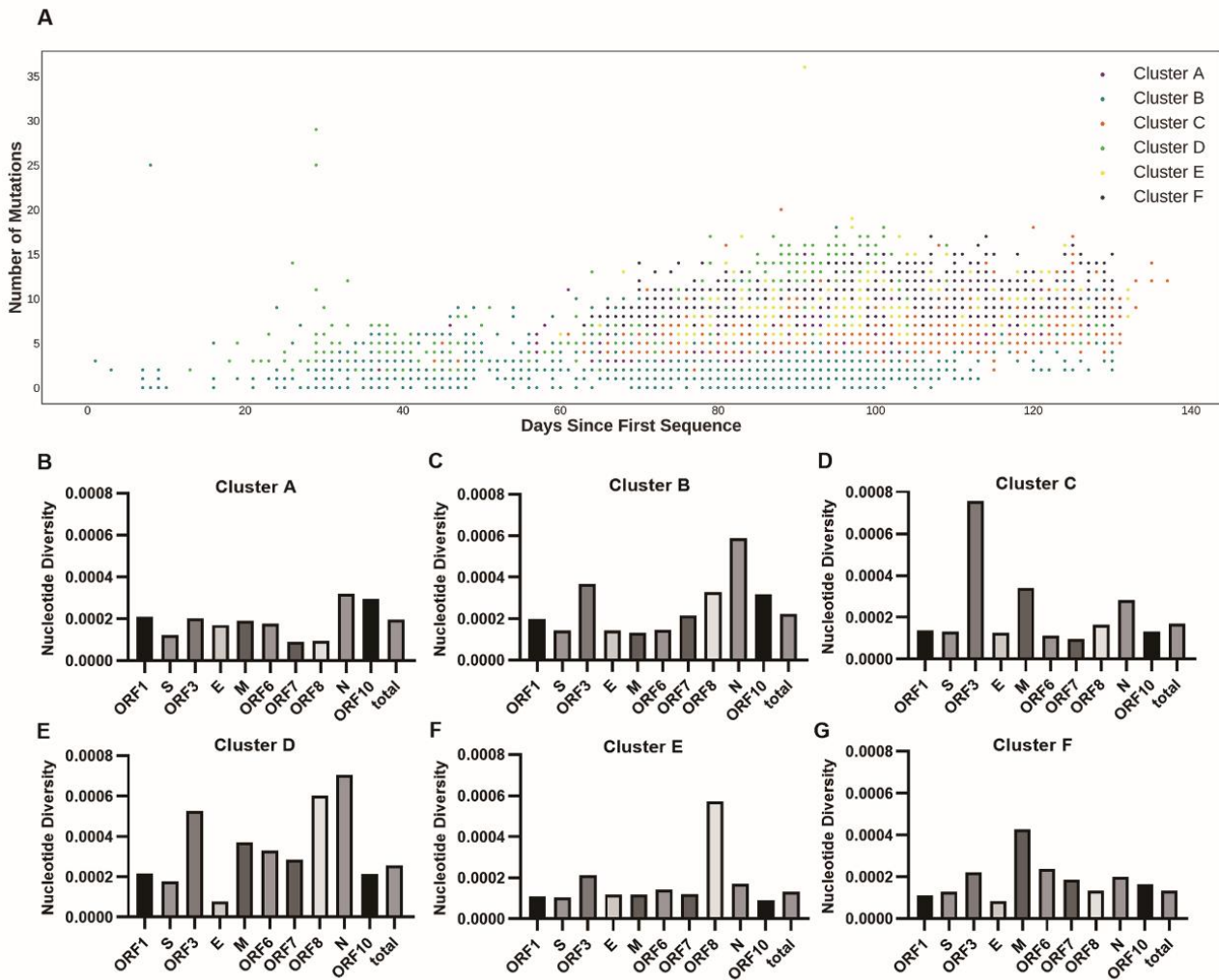


431

432 **Figure 2. Geographic distributions of the six clusters.** Pie charts display the proportions of six clusters among all SARS-

433 CoV-2 strains in each country. Circle sizes and the color scales correspond to the number of strains analyzed per country.

434



435

436 **Figure 3. The genetic diversity between clusters. (A)** The mutation counts over days of 16,873 SARS-CoV-2 strains. The

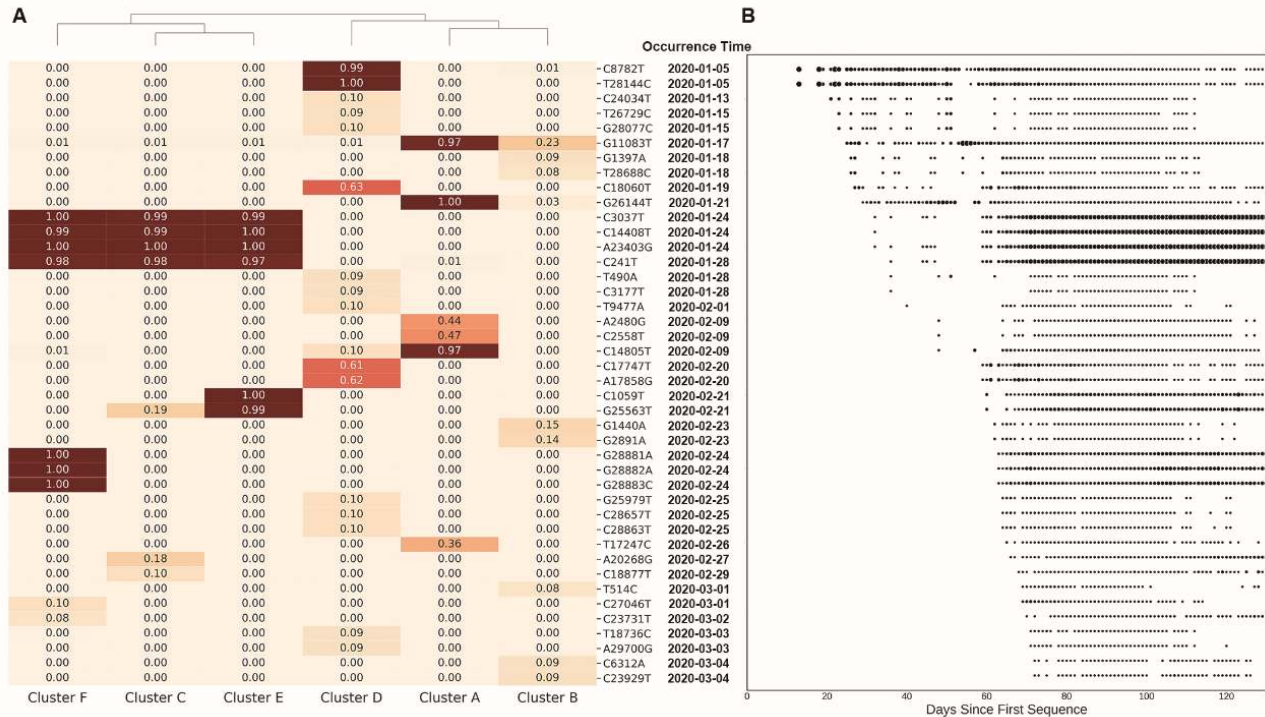
437 X axis represents the days from the corresponding collection date of strains to 24 December 2019 when the earliest strain

438 (EPI_ISL_402123) was collected. The Y axis represents the number of mutations of each collected strain. A mutation is

439 defined by a nucleotide change from the original nucleotide in the reference genome to the alternative nucleotide in the

440 studied viral genome. **(B-G)** The nucleotide diversity (π) per site for each gene and genome-wide across six clusters.

441



442

443 **Figure 4. The clustering of the six clusters by the extracted mutations. (A)** The heatmap displays mutation frequency

444 of the 42 mutations across six clusters. The colors and values represent different frequencies of the corresponding mutations

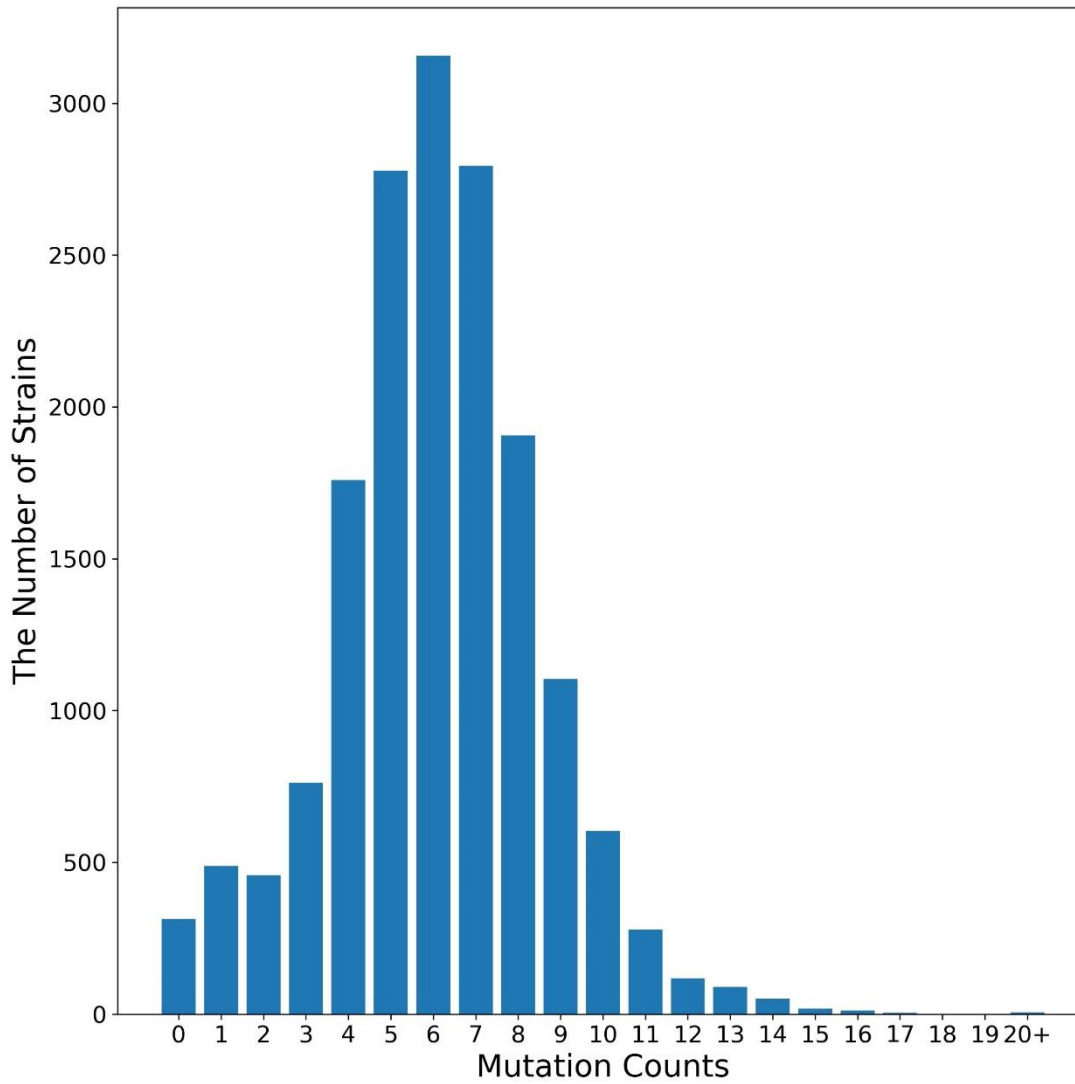
445 in each cluster. The collected days of the mutations are represented in (B). The X axis represents the days from the

446 corresponding collection date of strains to 24 December 2019 when the earliest strain (EPI_ISL_402123) was collected.

447 Circle sizes represent the frequency the of the mutations on each collection day.

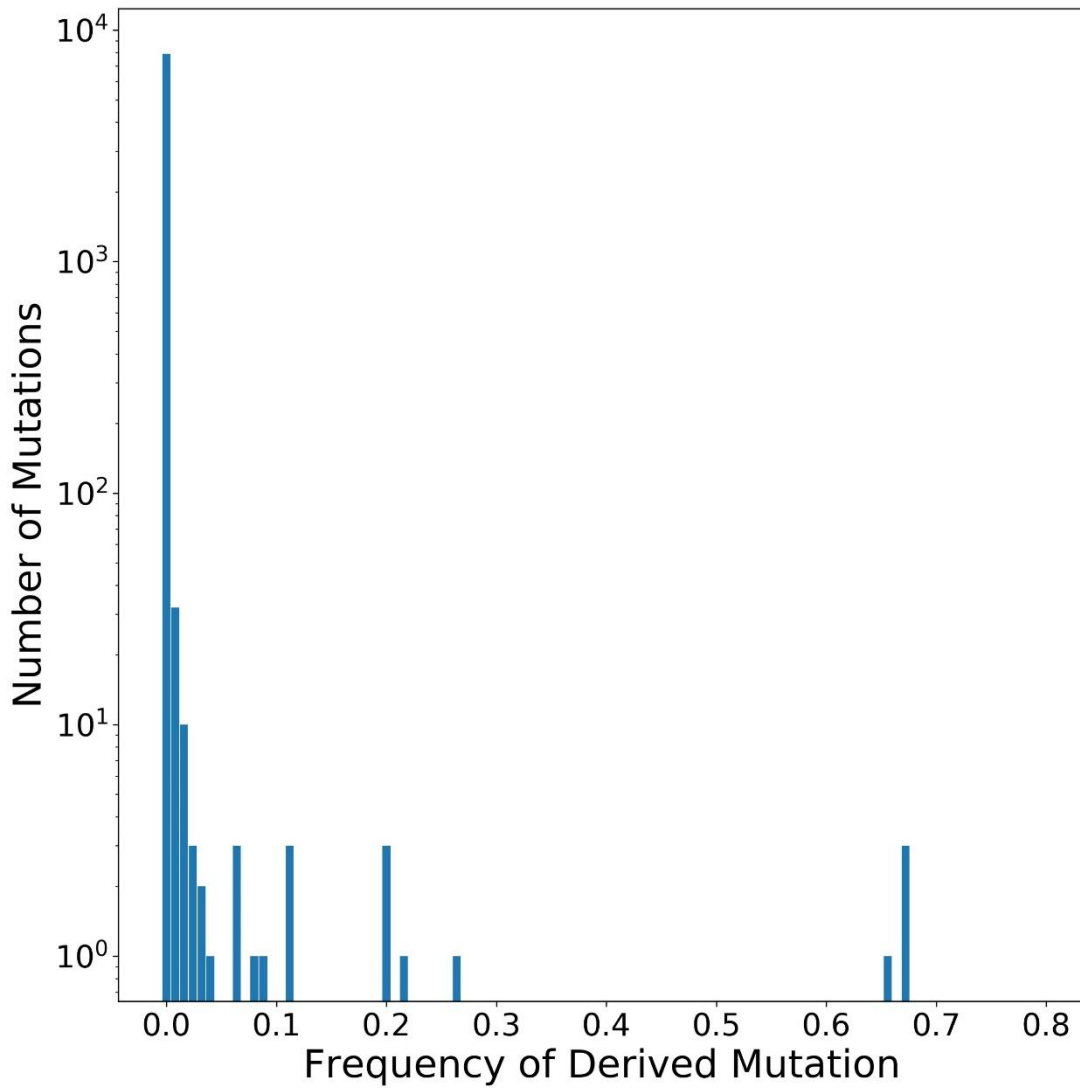
448

449 **Supplementary Information**



450
451 **Figure S1.** The distribution of the mutation counts of the 16,873 SARS-CoV-2 strains.

452



453

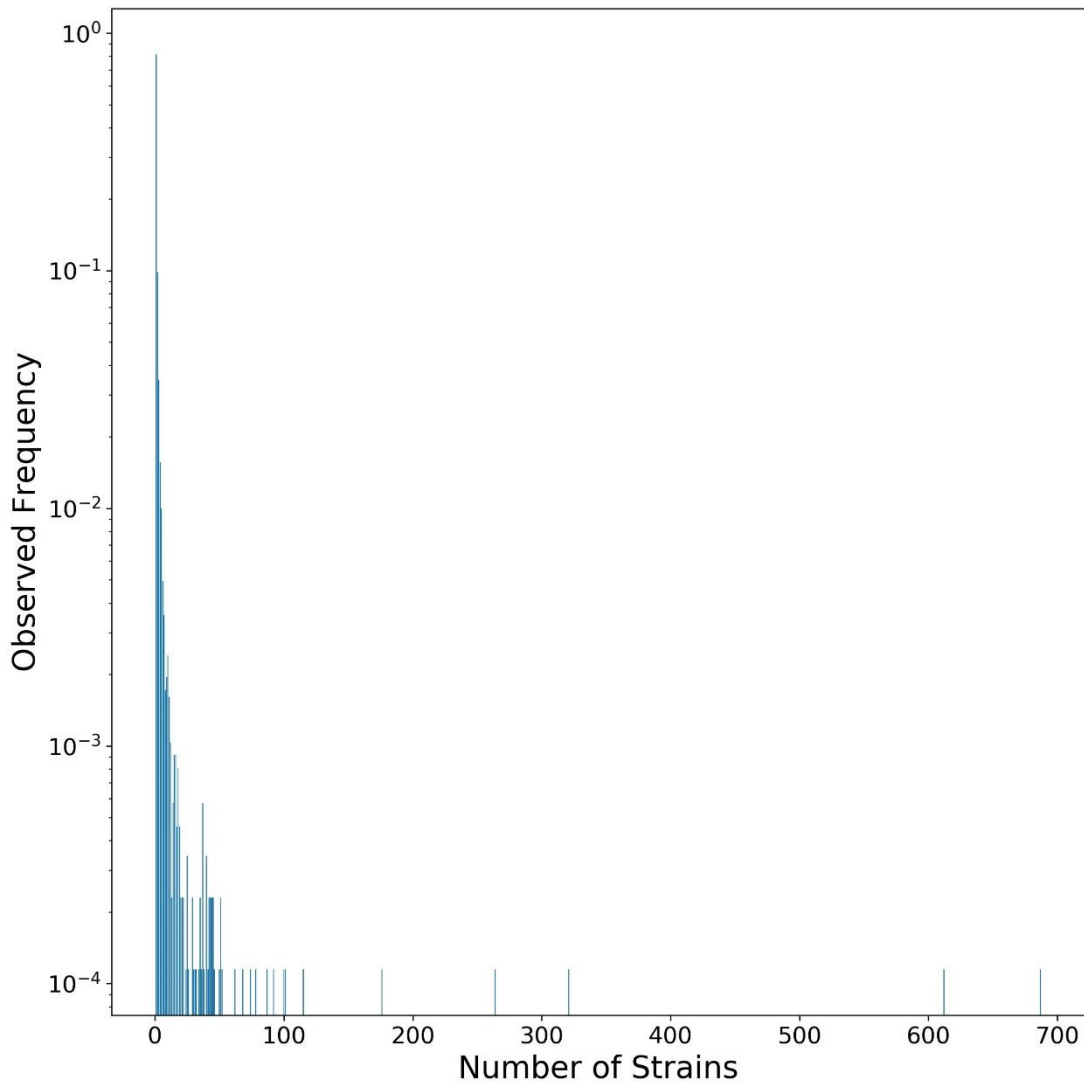
454

455 **Figure S2.** Frequency spectra of SARS-CoV-2. The mutation frequency of derived mutations of 16,873 SARS-CoV-2

456 stains is depicted on the X axis, and the number of mutations in which strains occurred is displayed on the Y axis. A log-

457 10 scale is used for the Y axis of the graph, and the Y axis ranges from 1 to 10,000.

458



459

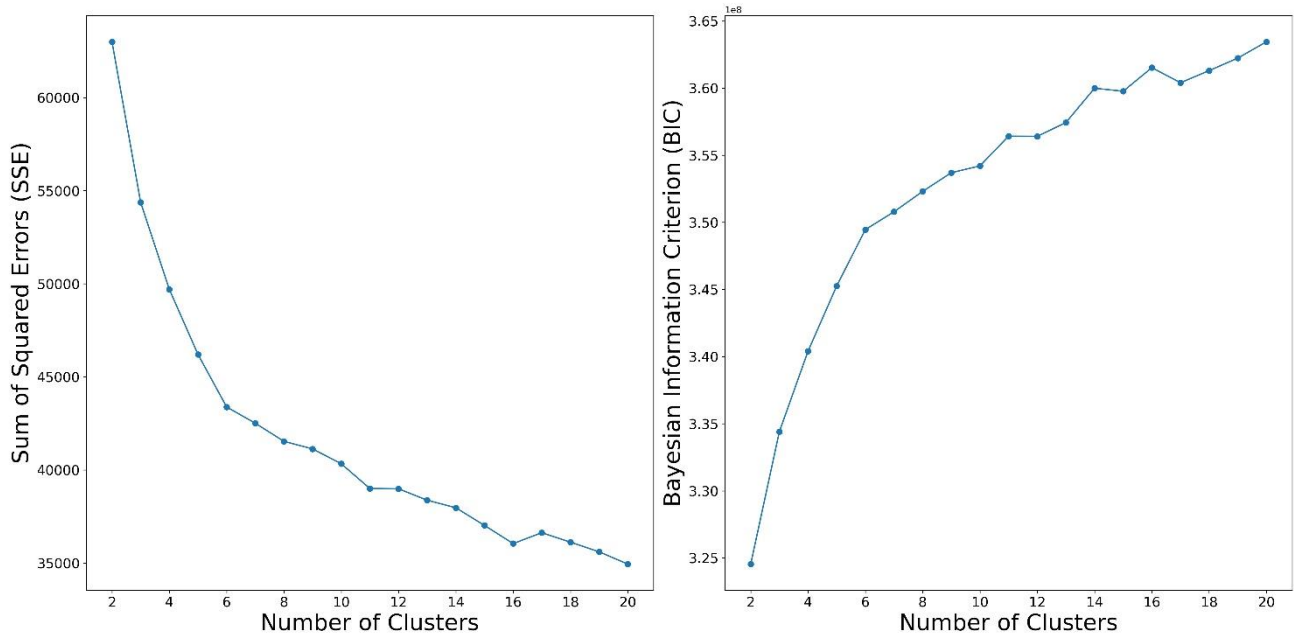
460

461 **Figure S3.** Normalized allele frequency of 16,873 SARS-CoV-2 strains. There are 8,706 unique genomes across the 16,873

462 strains. The X axis is the number of strains for each unique genome and the Y axis is the proportion of the unique genomes.

463 A log-10 scale is used for the Y axis of the graph, and the Y axis ranges from 0.0001 to 1.

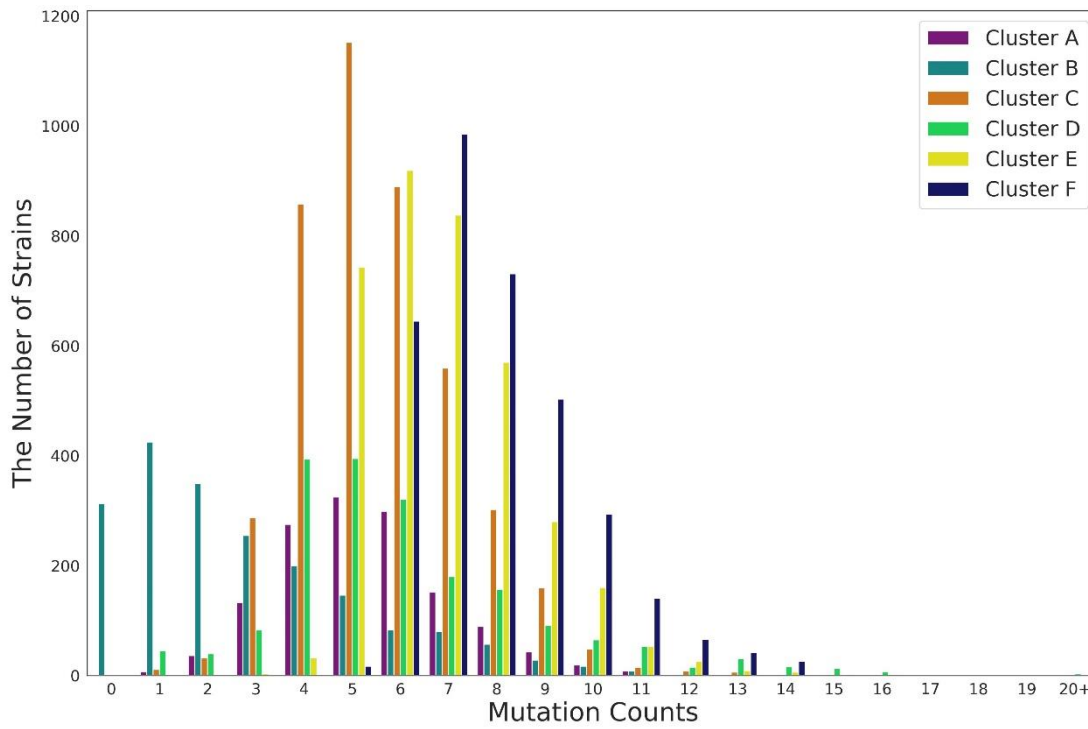
464



465

466 **Figure S4.** Evaluation of the number of clusters. The evolution of the sum of squared errors (SSE; left) and Bayesian
467 information criterion (BIC; right) for the number of clusters in the deep learning clustering runs. We used the elbow method
468 and chose the elbow of the curve as the number of clusters. The elbow method indicated that the number of clusters is six.

469

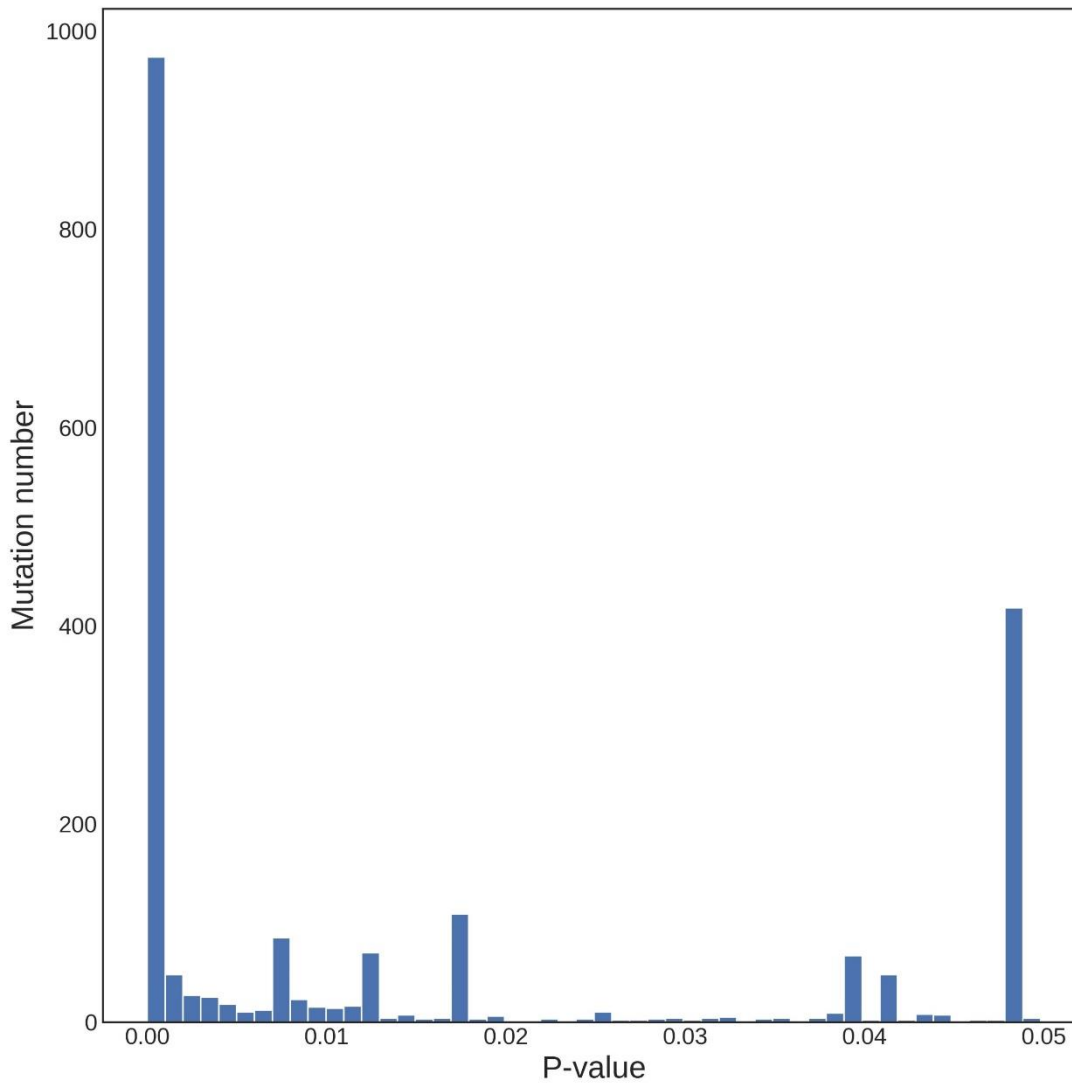


470

471

472 **Figure S5.** The distribution of the mutation counts of the strains for the six clusters.

473

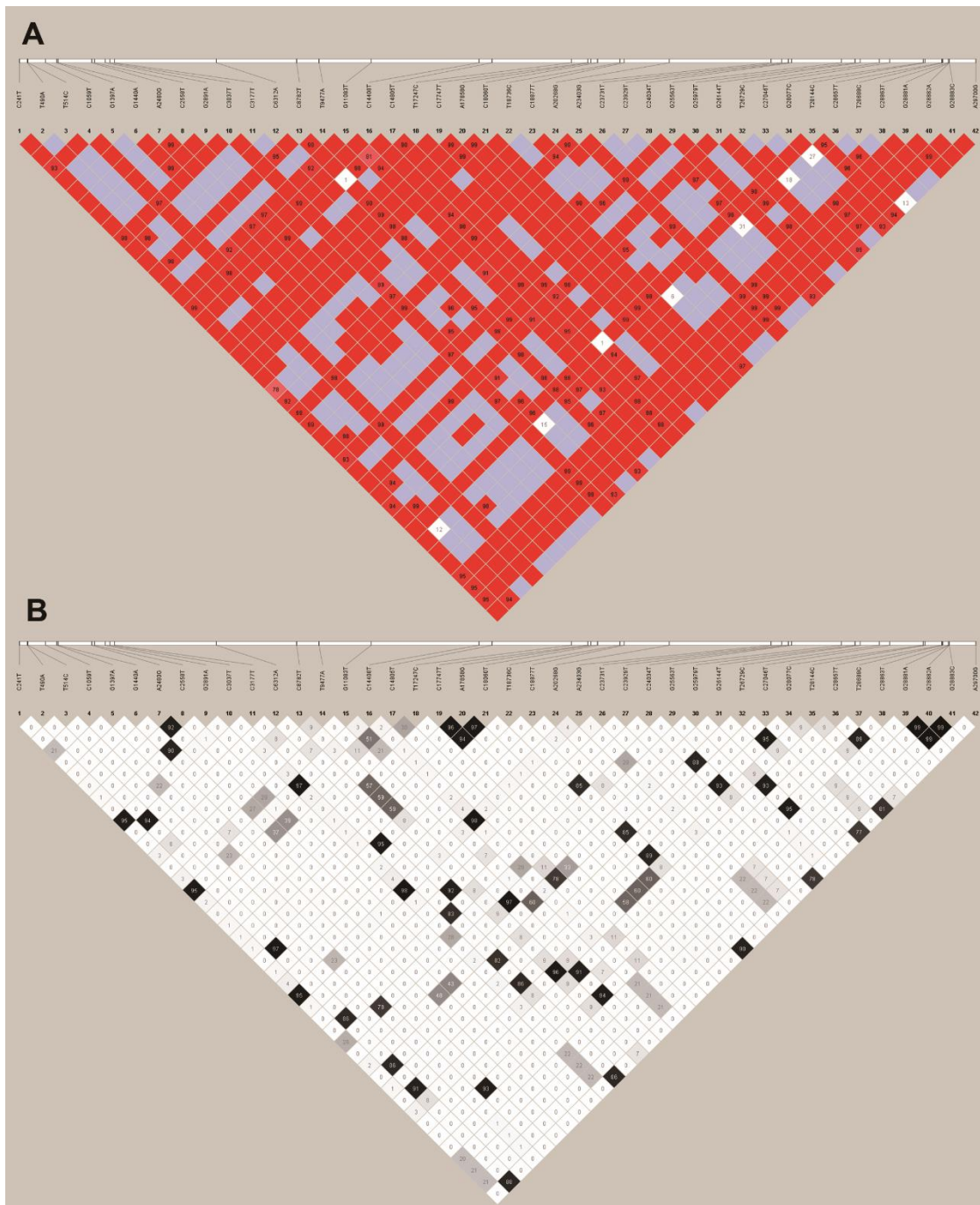


474

475

476 **Figure S6.** The distribution of P-values from the 2,094 mutations with P-values <0.05 by ANOVA.

477



478

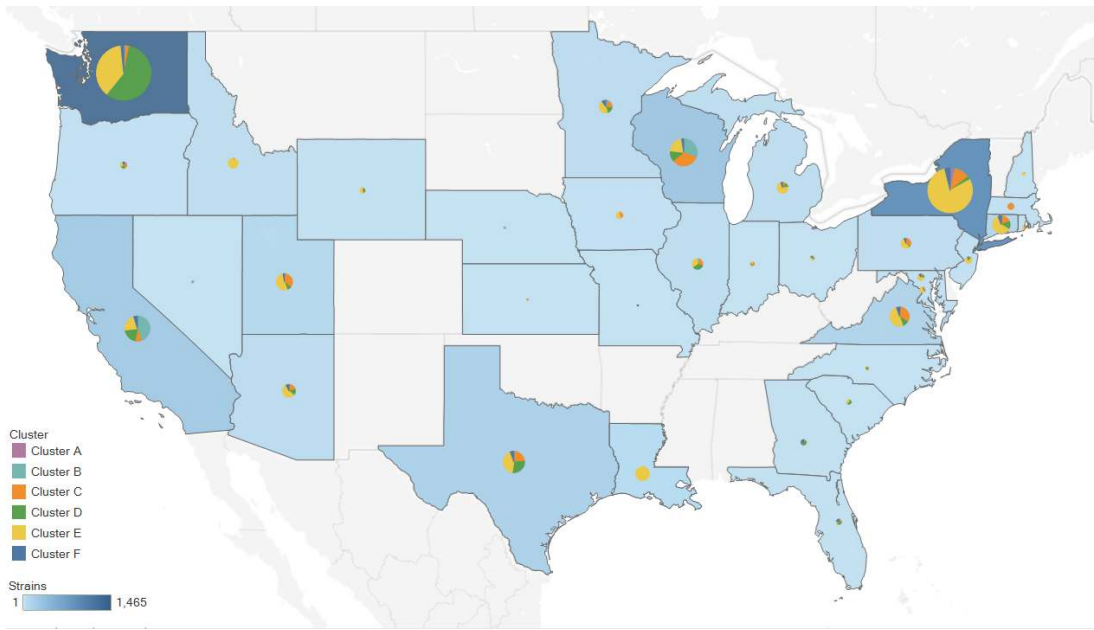
479 **Figure S7.** The D' and r^2 of the 42 mutations. (A) D' values that correspond to substitution pairs are expressed as

480 percentages and are shown within the respective squares. Higher D' values are indicated with a brighter red color. (B) The

481 numbers within the squares represent the r^2 scores for pairwise LD. r^2 values are represented by white for $r^2 = 0$, with

482 intermediate values for $0 < r^2 < 1$ indicated by shades of grey.

483



484

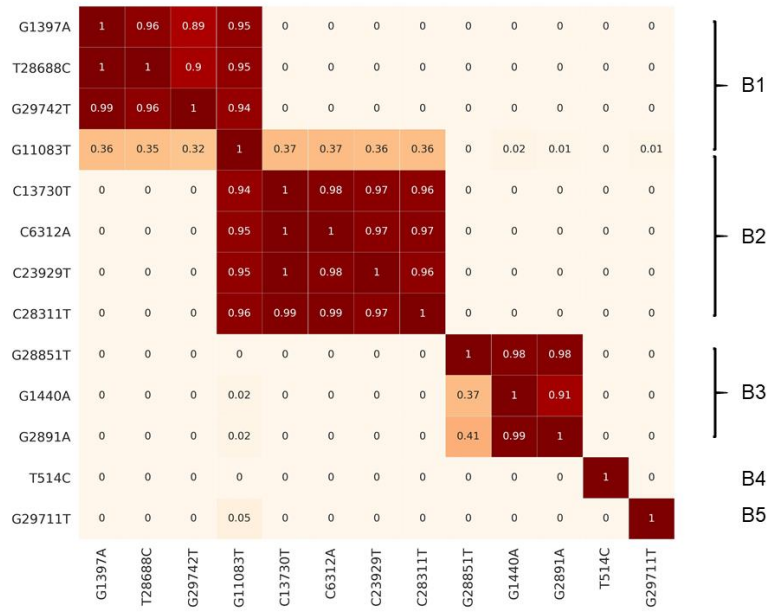
485

486 **Figure S8.** Geographic distribution of six clusters in the United States. Pie charts display the proportions of six clusters

487 among all SARS-CoV-2 strains in each state. Circle sizes and the color scales correspond to the number of strains analyzed

488 per state.

489



490

491

492 **Figure S9.** The pairwise dependency score (see Materials and Methods) of the mutations with frequency >0.05 within

493 cluster B. The heatmap shows that there are five major subclusters within cluster B.

494

495 **Table S1** Geographic distribution of six continents for each cluster.

Cluster	Cluster A	Cluster B	Cluster C	Cluster D	Cluster E	Cluster F	Total
Africa	3	4	65	7	10	9	98
Asia	38	648	248	217	57	116	1,324
Europe	1,137	990	3,119	212	1,108	2,961	9,527
North America	94	334	625	1,268	2,274	170	4,765
Oceania	110	161	233	196	191	149	1,040
South America	6	5	44	10	5	49	119
Total	1,388	2,142	4,334	1,910	3,645	3,454	16,873

496

497